

論文 / 著書情報
Article / Book Information

Title	Characterization of thiol-functionalized oligo(phenylene-ethynylene)-protected Au nanoparticles by scanning tunneling microscopy and spectroscopy
Authors	Hyunmo Koo,Shinya Kano,Daisuke Tanaka,Masanori Sakamoto,Toshiharu Teranishi,Gyoujin Cho,Yutaka Majima
Citation	Appl. Phys. Lett., Vol. 101, ,
Pub. date	2012, 8
URL	http://scitation.aip.org/content/aip/journal/apl
Copyright	Copyright (c) 2012 American Institute of Physics

Characterization of thiol-functionalized oligo(phenylene-ethynylene)-protected Au nanoparticles by scanning tunneling microscopy and spectroscopy

Hyunmo Koo, Shinya Kano, Daisuke Tanaka, Masanori Sakamoto, Toshiharu Teranishi et al.

Citation: *Appl. Phys. Lett.* **101**, 083115 (2012); doi: 10.1063/1.4747720

View online: <http://dx.doi.org/10.1063/1.4747720>

View Table of Contents: <http://apl.aip.org/resource/1/APPLAB/v101/i8>

Published by the American Institute of Physics.

Related Articles

Nanoimprint-lithography patterned epitaxial Fe nanowire arrays with misaligned magnetocrystalline and shape anisotropies

J. Appl. Phys. **113**, 17B502 (2013)

Cross-sectional sizes and emission wavelengths of regularly patterned GaN and core-shell InGaN/GaN quantum-well nanorod arrays

J. Appl. Phys. **113**, 054315 (2013)

Embedded mask patterning: A nanopatterning process to fabricate FePt magnetic media

Appl. Phys. Lett. **102**, 052406 (2013)

Nanostructured diamond-TiC composites with high fracture toughness

J. Appl. Phys. **113**, 043505 (2013)

From circular to triangular alumina nanopore arrays via simple replication

Appl. Phys. Lett. **102**, 021601 (2013)

Additional information on *Appl. Phys. Lett.*


Journal Homepage: <http://apl.aip.org/>

Journal Information: http://apl.aip.org/about/about_the_journal


Top downloads: http://apl.aip.org/features/most_downloaded

Information for Authors: <http://apl.aip.org/authors>

ADVERTISEMENT



Does your research require low temperatures? Contact Janis today.
Our engineers will assist you in choosing the best system for your application.



10 mK to 800 K
Cryocoolers
Dilution Refrigerator Systems
Micro-manipulated Probe Stations

LHe/LN₂ Cryostats
Magnet Systems

sales@janis.com www.janis.com
Click to view our product web page.

Characterization of thiol-functionalized oligo(phenylene-ethynylene)-protected Au nanoparticles by scanning tunneling microscopy and spectroscopy

Hyunmo Koo,¹ Shinya Kano,^{2,3} Daisuke Tanaka,^{3,4} Masanori Sakamoto,^{3,5,6}
Toshiharu Teranishi,^{3,4,5} Gyoujin Cho,¹ and Yutaka Majima^{1,2,3,a)}

¹Department of Printed Electronics Engineering, Sunchon National University, Sunchon 540-742, Korea

²Materials and Structures Laboratory, Tokyo Institute of Technology, Yokohama 226-8503, Japan

³CREST-JST, Yokohama 226-8503, Japan

⁴Graduate School of Pure and Applied Sciences, University of Tsukuba, Tsukuba 305-8571, Japan

⁵Institute for Chemical Research, Kyoto University, Uji 611-0011, Japan

⁶PRESTO-JST, Uji 611-0011, Japan

(Received 25 June 2012; accepted 8 August 2012; published online 23 August 2012)

The electrical properties of Au nanoparticles protected by thiol-functionalized oligo(phenylene-ethynylene) (OPE), 1,4-bis-(3-mercapto-phenylethynyl)benzene have been investigated by scanning tunneling microscopy (STM) and scanning tunneling spectroscopy (STS). The STM and scanning electron microscopy images of chemisorbed OPE-protected Au nanoparticles on Au(111) surface were similar, and the densities were almost identical. OPE-protected Au nanoparticles exhibited stochastic conductance switching behaviors, and current-voltage (I - V) and $\log I$ - V characteristics by STS at 100 K showed Coulomb blockade behaviors. The charging energy of Au nanoparticles was as high as 0.57 eV when the core diameter was 2.1 nm. Our results are significant for single-electron transistor memory applications. © 2012 American Institute of Physics. [<http://dx.doi.org/10.1063/1.4747720>]

Oligo(phenylene-ethynylene) (OPE) derivatives have attracted considerable attention owing to their potential applications to molecular devices due to their small highest occupied molecular orbital (HOMO)–lowest unoccupied molecular orbital (LUMO) gaps in molecules (~ 3 eV),¹ synthesis flexibility,^{2–6} negative differential resistance (NDR),^{7–10} and stochastic conductance switching phenomena.^{7,8,11–15} In particular, stochastic conductance switching phenomena have been intensively investigated using scanning tunneling microscopy (STM) because the origin of conductance switching in single OPE molecule is important for realizing single molecular switching devices. The origin of stochastic conductance switching phenomenon has been interpreted as the mobility of molecules,¹² conformational changes in molecules,¹³ bond hybridization,^{7,16,17} reductions in functional groups,¹⁸ functional group rotation,¹⁹ backbone phenyl ring rotations,²⁰ and intermolecular interactions.²¹

Au nanoparticles are one of the candidates for developing components of single-electron transistors because their core diameters can be controlled by chemical synthesis to be in the order of sub-nanometers, and the characteristics of Au nanoparticles can be functionalized by choosing adequate functional organic molecules as a ligand.^{22–26} Recently, our group found that OPE functional molecules can be applied to the ligand of Au nanoparticles and OPE-protected Au nanoparticles can be synthesized. Since these OPE-protected Au nanoparticles have promising applications to solid-state devices, it is desirable to examine their electrical properties.

In this paper, we describe our investigations into the electrical properties of OPE-protected Au nanoparticles by using STM. The density of OPE-protected Au nanoparticles is

discussed using STM and scanning electron microscopy (SEM). Stochastic conductance switching behaviors of OPE-protected Au nanoparticles are demonstrated by examining successive STM images. By using scanning tunneling spectroscopy (STS), we also demonstrate Coulomb blockade behaviors of OPE-protected Au nanoparticles observed in the current-voltage (I - V) characteristics at 100 K of a double-barrier tunneling junction (DBTJ) comprising tip/vacuum/OPE-protected Au nanoparticles/Au(111). We also evaluate the charging energy of Au nanoparticles and resistance of OPE ligands using orthodox theory and set-point current dependence of the resistance.

Au nanoparticles protected by OPE ligands were synthesized²⁷ and used as Coulomb islands of the DBTJ. From the transmission electron microscopy (TEM) image, the diameter of the Au core was evaluated as 2.1 nm. The chemical structure of the OPE ligand molecule is shown in Fig. 1(a). The Au substrate was prepared on cleaved mica using a vacuum evaporation method. Before the evaporation, mica was preheated at 580 °C for 11 h to remove contamination. After the thermal evaporation, the Au substrate was heated at 580 °C for 2 h to form a flat Au(111) surface. The substrate was immersed in a 0.16 nM dimethylformamide (DMF) solution of OPE-protected Au nanoparticles for 10 min. Finally, the substrate was rinsed with purified DMF to remove the excess OPE-Au nanoparticles. The sample was then introduced into ultrahigh vacuum STM [JEOL JSTM-4500 LT (modified)]. Figure 1(b) shows the schematic image of the DBTJ described in our work, which consists of a STM-tip/vacuum/OPE ligand/Au core/OPE ligand/Au(111) surface. The tunneling resistance R_1 between the STM tip and Au nanoparticle can be varied by adjusting the set-point current, while the resistance R_2 between the Au nanoparticle and Au(111) substrate depends on the OPE ligands. All the STM observations and STS measurements were carried out in the

^{a)}Author to whom correspondence should be addressed: Electronic mail: majima@msl.titech.ac.jp.

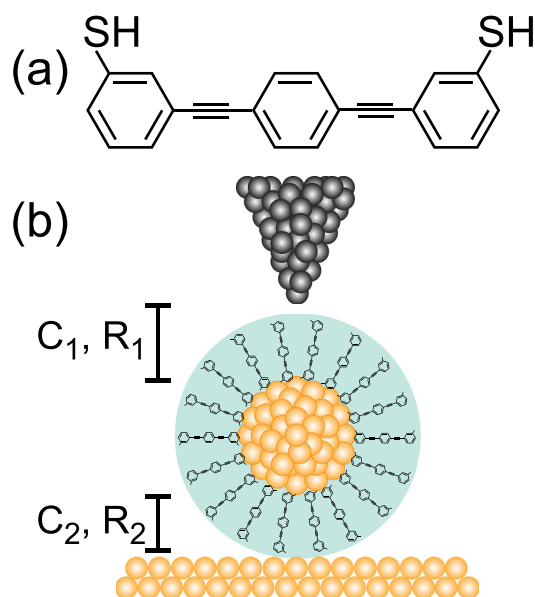


FIG. 1. (a) Chemical structure of thiol-functionalized OPE, 1,4-bis-(3-mercapto-phenylethynyl)benzene, ligand molecule. (b) Schematic drawing of the double-barrier tunneling junctions. Junction 1 is the tunneling barrier between STM-tip and Au core, which consists of a vacuum layer and OPE ligand, and junction 2 is the tunneling barrier between the Au core and Au(111) surface, which consists of only the OPE ligand.

ultrahigh vacuum STM at 100 K. An electrochemically etched tungsten tip was used, and the STM images were captured in a constant current mode. In the STS measurements, the sample bias voltage was swept within ± 2 V. The vacuum gap between the STM tip and OPE-Au nanoparticle was controlled by varying the set-point current from 10 pA to 1 nA.

To confirm the density of the OPE-protected Au nanoparticles on the Au(111) surface, SEM observations were performed by SU8000 (Hitachi High-Tech, Japan), which use 200 V as the landing voltage to observe the 2.1 nm-diameter Au core.

Figures 2(a)–2(c) are the SEM images of the sample that was prepared by immersion in the 0.16 nM DMF solution of OPE-protected Au nanoparticles for 10 min, and Figs. 2(d) and 2(e) are the STM images. Figures 2(b) and 2(c) are the magnified images of the square areas (A and B, respectively) shown in Fig. 2(a), and their image sizes are 150×150 and 100×100 nm², respectively, and identical to those of Figs. 2(d) and 2(e). The density of the OPE-protected Au nanoparticles in the SEM image is almost between 20 and 50 nanoparticles per 100×100 nm², and it is similar to that in the STM image. Consequently, the bright spots in the SEM and STM images are considered to be OPE-protected Au nanoparticles, and their density can be estimated by either of the two techniques, SEM or STM.

Figure 3(a) shows the STM image of OPE-protected Au nanoparticles on the Au(111) substrate, which was obtained with a sample bias voltage of -1.5 V, set-point current of 10 pA, and image size of 35×35 nm². The images (labeled as A–H) in Fig. 3(b) are successive images of OPE-protected Au nanoparticles, which were acquired at 7-, 15-, 25-, 32-, 47-, 59-, and 80-min intervals after image A was acquired. The stochastic switching phenomena of the OPE molecule have been studied previously in structures consisting of single and bundled OPE molecules in matrices of alkanethiol monolayers.^{7,11–14} Note that the stochastic conductance

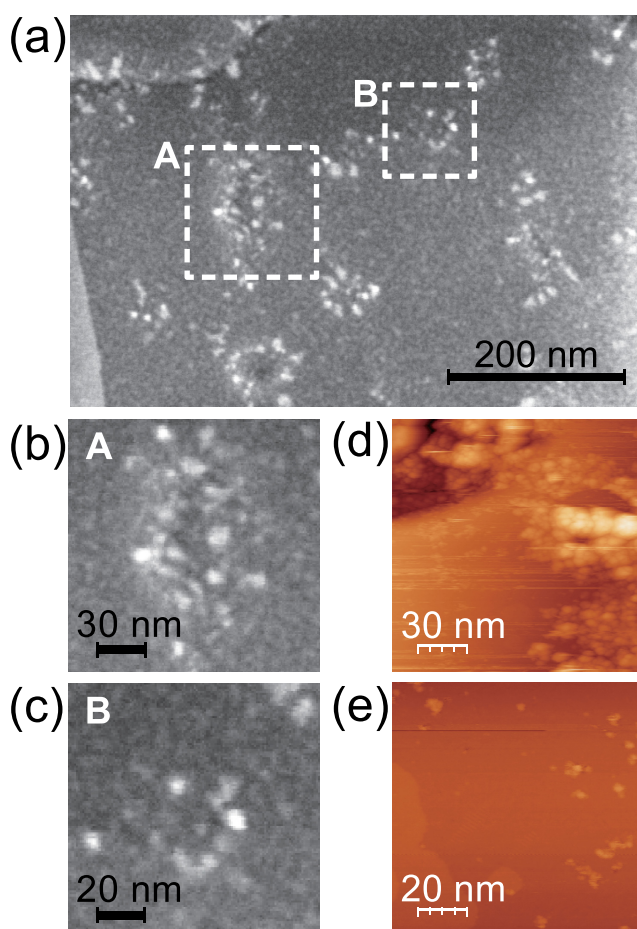


FIG. 2. Comparison between SEM and STM images of chemisorbed OPE-protected Au nanoparticles on Au(111) substrate. (a)–(c) and (d)–(e) are the SEM and STM images, respectively, of the sample prepared by immersion in a 0.16 nM DMF solution of OPE-protected Au nanoparticle for 10 min. (b) and (c) are magnified images of the square area (A and B, respectively) of (a). The size of (b) and (d) is 150×150 nm² and the size of (c) and (e) is 100×100 nm². The STM images for (d) and (e) were obtained with set-point currents of 20 pA and sample bias voltages of -1.8 V and 1.5 V, respectively.

switching phenomena have been observed even in OPE ligand-protected Au nanoparticles similar to OPE molecules.

In this study, referring to the high conductivity state as “ON” (A of Fig. 3(b)) and the low conductivity state as “OFF” (B of Fig. 3(b)), reversible switching between the ON and OFF states occurred for 80 min (ON-OFF-ON-OFF states). Figures 3(c) shows a cross-sectional profile of the OPE-protected Au nanoparticle shown as A and B in Fig. 3(b). The change in the height of Au nanoparticles was observed as conductance switching. Basically, the height information of Au nanoparticles in the STM image reflects the diameter of the Au nanoparticles.²⁸ However, the height of the Au nanoparticles appears smaller than the core diameter of Au nanoparticles in Fig. 3(c); this can be attributed to stochastic conductance switching phenomena, similar to those present in OPE molecules.

Figures 4(a)–4(f) show the linear plots and the corresponding semi-logarithmic plots for the experimental I – V characteristics (solid lines) of OPE-protected Au nanoparticles. These I – V curves were acquired for OPE-protected Au nanoparticles in the ON state by STS measurements at 100 K, since these nanoparticles were observed by STM images before and after the STS measurements. Coulomb blockade behaviors were observed repeatedly for set-point

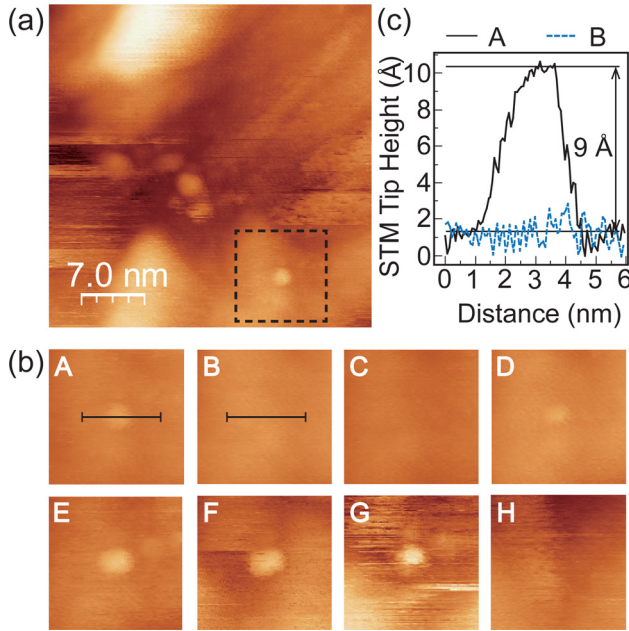


FIG. 3. Stochastic switching behaviors of OPE-protected Au nanoparticle, observed using STM. (a) STM images obtained with a sample bias voltage of -1.5 V, set point current of 10 pA, and image size of 35×35 nm 2 . (b) Successive STM images of single OPE-protected Au nanoparticle were acquired at 7-, 15-, 25-, 32-, 47-, 59-, and 80-min intervals from the image A. (c) is the cross-sectional profile of the Au nanoparticle in Fig. 3(b) (black solid lines and blue broken lines represent as A and B, respectively).

currents between 10 pA and 1 nA. The broken lines in Figs. 4(a)–4(f) show the theoretical curves fitted with the experimental results using the orthodox theory.^{25,26,29,30} The DBTJ parameters comprise resistance R_1 and capacitance C_1 between the STM tip and Au core, resistance R_2 and capacitance C_2 between the Au core and Au(111) substrate, and fractional residual charge Q_0 of the Au core, which can be estimated by using the orthodox theory.^{29,30}

The theoretical calculation process is shown as follows. According to the orthodox theory in DBTJ, the tunneling rate for the j th junction $\Gamma_j^\pm(n)$, where the \pm refers to the forward or reverse tunneling process across the junctions, can be derived from a basic golden-rule calculation.^{29,30}

$$\Gamma_j^\pm(n) = \frac{1}{R_j e^2} \left[\frac{-\Delta E_j^\pm}{1 - \exp(\Delta E_j^\pm / k_B T)} \right], \quad (1)$$

where ΔE_j^\pm is the energy change of the system when the electron tunnels across the j th tunneling barrier.

ΔE_j^\pm can be obtained from electrostatic energy considerations,

$$\Delta E_1^\pm = \frac{e}{C_1 + C_2} \left(\frac{e}{2} \pm (ne - Q_0) \pm C_2 V \right), \quad (2)$$

$$\Delta E_2^\pm = \frac{e}{C_1 + C_2} \left(\frac{e}{2} \pm (ne - Q_0) \mp C_1 V \right), \quad (3)$$

where e is the unit charge and V is the sample bias voltage. The ensemble distribution of the number of electrons on the nanoparticle $\sigma(n)$ is obtained by noting that the net probability for making a transition between any two adjacent states in steady state is zero as

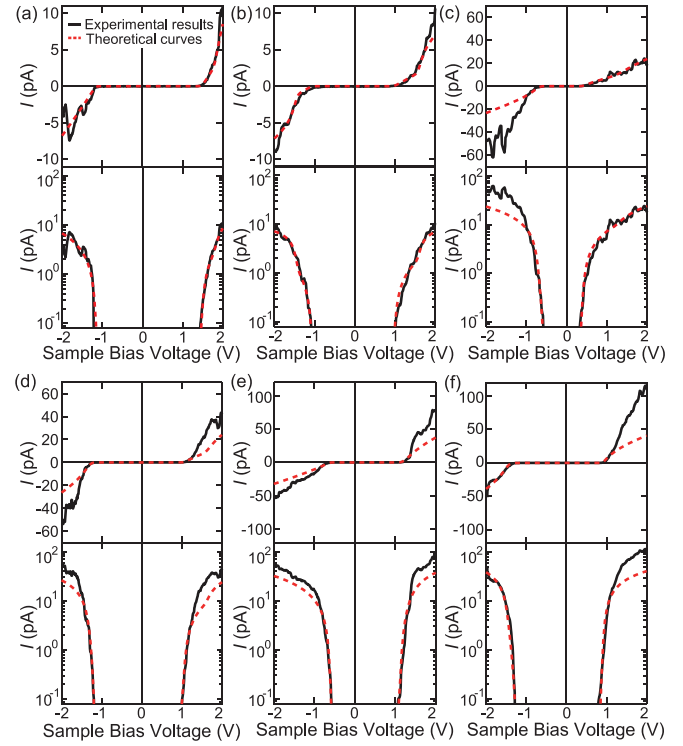


FIG. 4. Tunneling current versus sample bias voltage characteristics in STM-tip/vacuum/OPE ligand/Au core/OPE ligand/Au(111). (a)–(f) show the linear plots and the corresponding semi-logarithmic plots. Solid lines represent the experimental results and broken lines represent the theoretical $I(V)$ curves calculated using the orthodox theory. The values of the evaluated parameter are as follows: (a) $C_1 = 0.039$ aF, $C_2 = 0.062$ aF, $R_1 = 71$ G Ω , $R_2 = 12$ G Ω , and $Q_0 = -0.06e$; (b) $C_1 = 0.053$ aF, $C_2 = 0.079$ aF, $R_1 = 194$ G Ω , $R_2 = 11$ G Ω , and $Q_0 = -0.023e$; (c) $C_1 = 0.084$ aF, $C_2 = 0.15$ aF, $R_1 = 44.6$ G Ω , $R_2 = 15$ G Ω , and $Q_0 = -0.15e$; (d) $C_1 = 0.056$ aF, $C_2 = 0.067$ aF, $R_1 = 32$ G Ω , $R_2 = 10$ G Ω , and $Q_0 = -0.061e$; (e) $C_1 = 0.045$ aF, $C_2 = 0.091$ aF, $R_1 = 21.9$ G Ω , $R_2 = 8$ G Ω , and $Q_0 = 0.147e$; (f) $C_1 = 0.068$ aF, $C_2 = 0.046$ aF, $R_1 = 17.5$ G Ω , $R_2 = 7.5$ G Ω , and $Q_0 = 0.114e$, where e is the unit charge.

$$\sigma(n)[\Gamma_1^+(n) + \Gamma_2^+(n)] = \sigma(n+1)[\Gamma_1^-(n+1) + \Gamma_2^-(n+1)], \quad (4)$$

where $\sigma(n)$ is subjected to the normalization condition, $\sum_{n=-\infty}^{\infty} \sigma(n) = 1$.

Considering Eqs. (1)–(4), the total current through DBTJ is given by

$$\begin{aligned} I(V) &= e \sum_{n=-\infty}^{\infty} \sigma(n)[\Gamma_2^+(n) - \Gamma_2^-(n)] \\ &= e \sum_{n=-\infty}^{\infty} \sigma(n)[\Gamma_1^-(n) - \Gamma_1^+(n)]. \end{aligned} \quad (5)$$

In Figs. 4(a)–4(f), the theoretical $I(V)$ are shown as broken lines, which were numerically calculated by Eq. (5). The theoretical curves are fitted to the onset of the first Coulomb steps in the experimental STS results. The estimated DBTJ parameters are shown in the caption of Fig. 4. It notes that the experimental results agree well with the theoretical $I(V)$ curves within the sample bias voltage region between -1 and 1 V. On the contrary, the experimental results sometimes larger than the theoretical $I(V)$ curves due to a nonlinearity of I – V characteristics with respect to the sample bias voltage region higher than ± 1.0 V.²⁶

Considering the mirror image of a point charge model between a charged sphere and a conducting plate, the capacitance between the Au nanoparticle and conducting plate of the Au substrate (or the STM tip) is proportional to $4\pi\epsilon_0\epsilon_r r$, where ϵ_0 is the dielectric constant of vacuum; ϵ_r , the relative dielectric constant; and r , the diameter of the Au nanoparticle.^{26,30,31} If we assume the relative dielectric constant of vacuum ($\epsilon_r = 1$) and $r = 1.05$ nm, the estimated capacitance between the Au nanoparticle and conducting plate (C) is 0.12 aF. The electrostatic charging energy of the Au nanoparticle is $E_c = e^2/2C_\Sigma$, where C_Σ is the sum of the capacitances of the DBTJ. If C_Σ is assumed as $2C$, the estimated E_c is 0.34 eV. The experimental average E_c for 22 of the STS measurements is 0.57 eV, which is of the same order as the estimated value of 0.34 eV. Because E_c is considerably larger than the thermal fluctuation $k_B T$ (~ 9 meV), Coulomb blockade behaviors are clearly observed at 100 K in Figs. 4(a)–4(f). Since the charging energy of 0.57 eV is 20 times greater than $k_B T$ at room temperature, there exists the possibility that this OPE-protected Au nanoparticle can be used as a Coulomb island in the single-electron transistor operating at room temperature.²⁶

Figure 5(a) shows the relationship between R_1 and the set-point current (I_{set}). The solid straight line represents the measurement conditions when $I_{\text{set}}R_1 = 2$ V. In Fig. 5(a), R_1 is inversely proportional to I_{set} , which indicates that the distance between the STM tip and Au core is dependent on I_{set} . Figure 5(b) shows the relationship between R_2 and I_{set} . The solid straight line represents the R_2 value when $I_{\text{set}}R_1 = 2$ V ($R_1/R_2 = 1$), and the dotted straight line represents the R_2 value when $I_{\text{set}}R_1 = 0.04$ V ($R_1/R_2 = 50$). If the R_1/R_2 ratio is less than 50, the R_2 value can be defined by fitting the theoretical curve to the experimental I – V curve, especially at the onset of the first Coulomb steps of both bias voltage polarities. We have reported the R_2 dependence of alkanethiol-protected and basic-ligand-protected Au nanoparticles previously and demonstrated that the R_2 value is independent of I_{set} when $R_1/R_2 > 1$.^{26,30} The constant value of R_2 is determined by the ligand molecule between the Au core and Au(111) substrate on the basis of the DBTJ structure in Fig. 1(b). In Fig. 5(b), R_2 is independent of I_{set} when $I_{\text{set}} \leq 20$ pA and dependent on I_{set} when $I_{\text{set}} \geq 50$ pA. Hence, R_2 of the OPE ligand molecule is determined to be 15.0 G Ω from the average value of R_2 when $I_{\text{set}} \leq 20$ pA. When $I_{\text{set}} \geq 50$ pA, the R_2 value is inversely proportional to I_{set} , which indicates that the STM tip contacted the OPE-protected Au nanoparticle. Since the height of the OPE-protected nanoparticle at the OFF state is lower than that at the ON state, the conductance of the OFF state should be smaller than that of the ON state. The R_2 evaluation at the OFF state and the applications of OPE-Au nanoparticles to single-electron transistors will be reported in the next paper.

In this paper, we have described our investigations into the electrical properties of chemically synthesized Au nanoparticles protected by OPE ligand molecules. Stochastic conductance switching behaviors were observed in the case of chemisorbed OPE-protected Au nanoparticles by STM analyses; this is similar to the behavior of individual OPE molecules. Coulomb blockade behaviors were also observed in

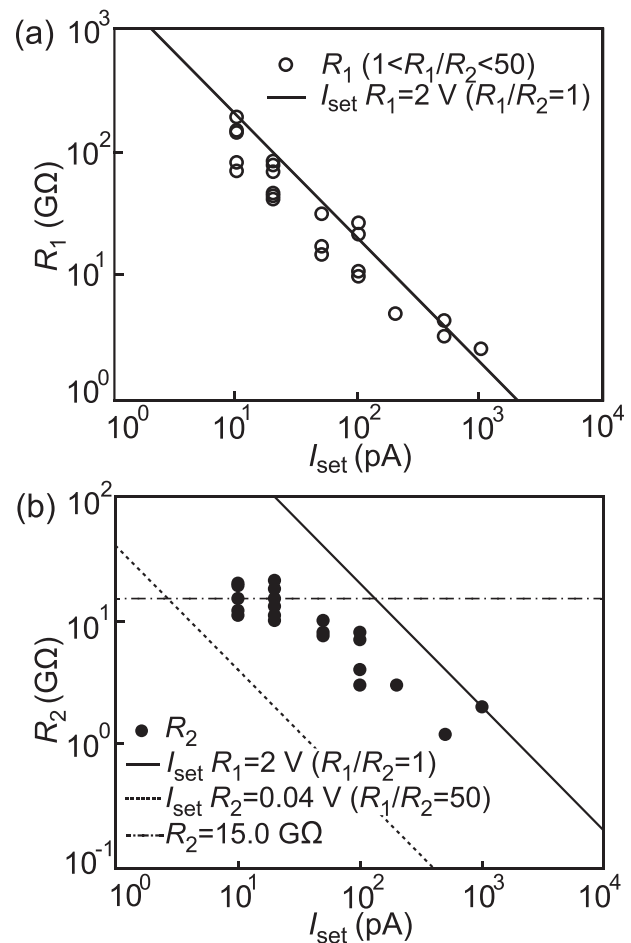


FIG. 5. Set-point current (I_{set}) dependence of tunneling resistances (a) R_1 , and (b) R_2 for OPE-protected Au nanoparticles. Open and closed circles represent the evaluated values of R_1 and R_2 , respectively. (a) Solid line indicates the power law $R_1 \propto 1/I_{\text{set}}$ when $I_{\text{set}}R_1 = 2$ V. (b) The solid and the dashed lines show the power law relationship $I_{\text{set}}R_1 = 2$ V ($R_1/R_2 = 1$) and $I_{\text{set}}R_1 = 0.04$ V ($R_1/R_2 = 50$), respectively. The average values of R_2 for OPE-protected Au nanoparticles are 15 G Ω when $I_{\text{set}} \leq 20$ pA.

current-voltage (I – V) and log I – V characteristics by STS analyses at 100 K; the charging energy of Au nanoparticle was estimated to be 0.57 eV when the core diameter was 2.1 nm. The resistance of the OPE ligand molecule was 15 G Ω in the ON states. Our results are significant for applications to single-electron transistor memories operating at room temperatures due to the stochastic switching of the OPE ligand molecules.

We thank M. Miyakawa for providing technical support for SEM observations. This study was partially supported by a Grant-in-Aid for Scientific Research on Innovative Areas (No. 20108011, π -Space) from the Ministry of Education, Culture, Sports, Science and Technology (MEXT), Japan; a Grant-in-Aid for Scientific Research (A) (23245028) from MEXT (T.T.); a Grant-in-Aid for Japan Society for the Promotion of Science (JSPS) Fellows (No. 11J08966) from MEXT (S.K.); the Collaborative Research Program of Institute for Chemical Research, Kyoto University (#2012-63); the Collaborative Research Project of Materials and Structures Laboratory, Tokyo Institute of Technology; and the World Class University (WCU) Program through the Ministry of Education, Science and Technology of Korea (R31-10022).

- ¹X. Xiao, L. A. Nagahara, A. M. Rawlett, and N. Tao, *J. Am. Chem. Soc.* **127**, 9235 (2005).
- ²Y. Luo, C.-K. Wang, and Y. Fu, *J. Chem. Phys.* **117**, 10283 (2002).
- ³Y. Selzer, A. Salomon, J. Ghabboun, and D. Cahen, *Angew. Chem., Int. Ed.* **41**, 827 (2002).
- ⁴C. W. Bauschlicher, J. W. Lawson, A. Ricca, Y. Xue, and M. A. Ratner, *Chem. Phys. Lett.* **388**, 427 (2004).
- ⁵J. Taylor, M. Brandbyge, and K. Stokbro, *Phys. Rev. B* **68**, 121101 (2003).
- ⁶N. Vedova-Brook, N. Matsunaga, and K. Sohlberg, *Chem. Phys.* **299**, 89 (2004).
- ⁷P. A. Lewis, C. E. Inman, F. Maya, J. M. Tour, J. E. Hutchison, and P. S. Weiss, *J. Am. Chem. Soc.* **127**, 17421 (2005).
- ⁸S. Yeganeh, M. Galperin, and M. A. Ratner, *J. Am. Chem. Soc.* **129**, 13313 (2007).
- ⁹J. D. Le, Y. He, T. R. Hoye, C. C. Mead, and R. A. Kiehl, *Appl. Phys. Lett.* **83**, 5518 (2003).
- ¹⁰K. Walzer, E. Marx, N. C. Greenham, R. J. Less, P. R. Raithby, and K. Stokbro, *J. Am. Chem. Soc.* **126**, 1229 (2004).
- ¹¹K.-H. Jung, E. Hase, Y. Yasutake, H.-K. Shin, Y.-S. Kwon, and Y. Majima, *Jpn. J. Appl. Phys. Part 2* **45**, L840 (2006).
- ¹²G. K. Ramachandran, T. J. Hopson, A. M. Rawlett, L. A. Nagahara, A. Primak, and S. M. Lindsay, *Science* **300**, 1413 (2003).
- ¹³Z. J. Donhauser, B. A. Mantooth, K. F. Kelly, L. A. Bumm, D. J. Monnell, J. J. Stapleton, D. W. Price, Jr., A. M. Rawlett, D. L. Allara, J. M. Tour, and P. S. Weiss, *Science* **292**, 2303 (2001).
- ¹⁴P. A. Lewis, C. E. Inman, Y. Yao, J. M. Tour, J. E. Hutchison, and P. S. Weiss, *J. Am. Chem. Soc.* **126**, 12214 (2004).
- ¹⁵N. Majumdar, N. Gergel-Hackett, J. C. Bean, L. R. Harriott, G. Pattanaik, G. Zangari, Y. Yao, and J. M. Tour, *J. Electron. Mater.* **35**, 140 (2006).
- ¹⁶A. M. Moore, A. A. Dameron, B. A. Mantooth, R. K. Smith, D. J. Fuchs, J. W. Ciszek, F. Maya, Y. Yao, J. M. Tour, and P. S. Weiss, *J. Am. Chem. Soc.* **128**, 1959 (2006).
- ¹⁷H. Sellers, A. Ulman, Y. Shnidman, and J. E. Eilers, *J. Am. Chem. Soc.* **115**, 9389 (1993).
- ¹⁸J. M. Seminario, A. G. Zacarias, and J. M. Tour, *J. Am. Chem. Soc.* **122**, 3015 (2000).
- ¹⁹M. D. Ventra, S.-G. Kim, S. T. Pantelides, and N. D. Lang, *Phys. Rev. Lett.* **86**, 288 (2001).
- ²⁰J. M. Seminario, P. A. Derosa, and J. L. Bastos, *J. Am. Chem. Soc.* **124**, 10266 (2002).
- ²¹N. D. Lang and Ph. Avouris, *Phys. Rev. B* **62**, 7325 (2000).
- ²²T. Teranishi, *C. R. Chim.* **6**, 979 (2003).
- ²³A. Zabet-Khosousi and A.-A. Dhirani, *Chem. Rev.* **108**, 4072 (2008).
- ²⁴N. Okabayashi, K. Maeda, T. Muraki, D. Tanaka, M. Sakamoto, T. Teranishi, and Y. Majima, *Appl. Phys. Lett.* **100**, 033101 (2012).
- ²⁵X. Li, Y. Yasutake, K. Kono, M. Kanehara, T. Teranishi, and Y. Majima, *Jpn. J. Appl. Phys. Part 1* **48**, 04C180 (2009).
- ²⁶S. Kano, Y. Azuma, M. Kanehara, T. Teranishi, and Y. Majima, *Appl. Phys. Express* **3**, 105003 (2010).
- ²⁷M. Sakamoto, D. Tanaka, and T. Teranishi, "Rigid Bidentate Ligands Focus the Size of Gold Nanoparticle" (submitted).
- ²⁸M. Sakamoto, D. Tanaka, H. Tsunoyama, T. Tsukuda, Y. Minagawa, Y. Majima, and T. Teranishi, *J. Am. Chem. Soc.* **134**, 816 (2012).
- ²⁹A. E. Hanna and M. Tinkham, *Phys. Rev. B* **44**, 5919 (1991).
- ³⁰H. Zhang, Y. Yasutake, Y. Shichibu, T. Teranishi, and Y. Majima, *Phys. Rev. B* **72**, 205441 (2005).
- ³¹S. Kano, Y. Yamada, K. Tanaka, and Y. Majima, *Appl. Phys. Lett.* **100**, 053101 (2012).